JOURNAL OF GUIDANCE, CONTROL, AND DYNAMICS
Vol. 26, No. 5, September–October 2003

# Planning Algorithm for Multiple Satellite Clusters

Mark E. Campbell*
*Cornell University, Ithaca, New York 14853*

**A generalized planning methodology for satellite clusters is proposed. The methodology utilizes Hamilton–Jacobi–Bellman optimality (minimum time or minimum fuel) to generate quickly a set of maneuvers from an initial stable formation to a final stable formation. Maneuvers are selected from the original set based on the maneuver time, fuel, and collision proximity. The final maneuvers are calculated by optimizing the switch times using a realistic set of orbital dynamics. The algorithm is developed to be distributed and scales well as the number of satellites increases. A minimal level of communication is used because only switch times and collision proximity information are distributed from the planner. An example with four satellites maneuvering in an eccentric orbit ($e = 0.2$) is presented. Results show that optimal cluster maneuvers (minimum time or minimum fuel) can be generated within minutes, and most of the computational implementation can be accomplished in parallel.**

## I. Introduction

SATELLITE clusters are envisioned as an enabling technology for defense- and science-based missions. NASA's Origins program is planning a series of missions that perform spaceborne interferometry to image far off planets for possible life forms.[1] The U.S. Air Force is planning a distributed space-based, synthetic aperture radar mission within the next few years, possibly followed by a full deployment.[2] In each case, clusters of satellites hold the promise of increasing performance and reliability through distribution, while decreasing cost. The latter is a key aspect that will rely on levels of autonomous control algorithms and software currently being developed.

The challenge of ensuring these clusters are a safe reality is large. Precision sensing, such as global positioning systems[3] or local navigation systems,[4] is required to maintain performance for science and to prevent collisions.[5] For many applications, such as distributed space-based radar,[2] the relative separation of the satellites can vary from 250 down to 10 m. Low-thrust, high specific impulse propulsion[6,7] is required to allow maneuvering to many configurations and station keeping to maintain formation. Distributed communication[8] and computer architectures are required to reduce operations and utilize autonomy.[9,10]

Figure 1 shows a typical control architecture for distributed satellites. Shown is a formation control loop for each spacecraft, with a spacecraft-level trajectory planner, control algorithm/logic, and estimation and sensing. Estimated or sensed information is usually shared (simplex for leader–follower or duplex for more complex architectures) such that each satellite has sufficient knowledge to develop its own plan. Control logic includes model-based feedback[11] or feedforward control.[12] The relative dynamics between the satellites are usually sufficiently slow to allow effective model-predictive control techniques (feedforward) that work quite well. This may be shown by deleting the connection between estimation and control blocks in each spacecraft loop of Fig. 1.

Planning for the cluster includes reconfiguration of the cluster from one stable formation to another; in the case of feedforward control, the planner can also include maintenance of the stable formation by rejecting disturbances. Portions of the satellite planner(s) can be distributed; therefore, it is shown as two blocks: a fleet-level planner and a spacecraft-level planner. The fleet planner makes global decisions, including relative locations, timing, and constraints for each of the satellites to 1) coordinate for science, 2) maintain the health of the fleet, and 3) prevent collisions. Spacecraft-level planners receive the assignment and constraints from the fleet planner and plan the specific trajectory to be implemented.

Much work on distributed satellite systems has focused on smaller clusters containing 2–3 satellites. As the science-based missions and the underlying technology mature, larger clusters (8–16 or more) are envisioned.[13] It is important during this process to develop algorithms, software, and architectures that scale well with the number of satellites. Common attributes of scaled systems include distributed and flexible computation, system reliability, and minimized communications. In addition, the algorithms could be adaptable such that those satellites with more capability can take on more of a computational burden.

The objective of this work is to develop a fleet and spacecraft planning methodology that specifically addresses the important requirements of future satellite cluster based missions. These include minimal communications, typical of architectures that scale well with $n$ spacecraft; distributed computation, typical of hierarchical and parallel architectures that scale well with $n$ spacecraft; optimality, in the sense of minimum fuel/time for each spacecraft and across the cluster; reliability, including preventing collisions; compatibility, with state of the art, low-impulse electric propulsion; and realism, with working solutions that include nonidealities such as $J_2$ effects and orbit eccentricity.

Many current approaches map well onto several of these challenges, but not to others. Carpenter's decentralized control[14] assumes the use of a planner and does not develop a planner specifically. Advantages of this approach are its full-state optimal control with a minimum level of communication between satellites. Disadvantages include the level of computation, communications, and fuel as $n$ increases; said another way, as $n$ increases, control places more of a burden on the communication and computation. Note also that fuel usage is currently one of the primary road blocks between distributed satellite research and realistic systems, and feedback control typically uses more fuel than planned, minimum-fuel maneuvers. Controllers that specifically take into account the effects of the $J_2$ gravity perturbation[11,15] have also been developed; this works well for small clusters, but again develops communication and computation problems as $n$ increases. For variable specific-impulse thrusters, Yang et al.[16] have developed a fuel-optimal planner using a genetic search algorithm. There is also a large body of research in the areas of single-satellite orbital control and rendezvous,[17] but it is unclear how these algorithms scale to large numbers of satellites. Carter and Humi[18] developed fuel-optimal rendezvous trajectories for norm-bounded thrusters. The work closest to the approach presented here is by Tillerson et al.[12] This work uses a linear program (LP) to find minimum time/fuel maneuvers, including $\Delta V$ maps and complex trajectories. Schetter et al.,[10] in similar work, used the

Received 15 July 2002; revision received 28 February 2003; accepted for publication 5 March 2003. 

*Assistant Professor, Department of Mechanical and Aerospace Engineering, 208 Upson Hall; mc288@cornell.edu. Senior Member AIAA.

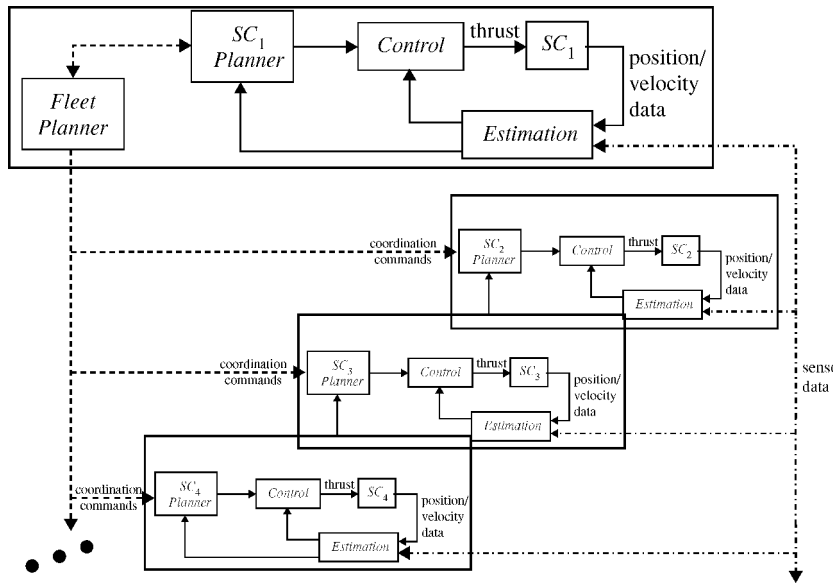


**Fig. 1 Architecture for distributed satellite systems, showing distributed planning and sensing.**

LP and a bidding mechanism to select the appropriate final satellite locations. Inalhan et al.[19] have extended this work to include noncircular orbits and collision avoidance.

The approach here is to use an optimal-time/fuel solution for an individual satellite within the cluster as a basis and to build a methodology to include collision avoidance, realistic dynamics, and cluster optimality. The primary advantages of this approach compared to that of the LP and other approaches are that 1) it can be verified to be optimal at the spacecraft and fleet levels, 2) the satellites communicate/share switching times rather than maneuver trajectories, thus reducing communication load, and 3) collision avoidance is addressed by varying the maneuver initial and final times, thus utilizing optimal control and the base orbital dynamics. The current disadvantage of the approach here is guaranteed convergence for maneuvers that are more general (many control inputs, more than one orbit in length). As will be shown, the initial switch times can be found very quickly and reliably for many common architectures, and optimality can easily be evaluated.

This paper is organized as follows. First, the overall planner methodology is presented. This is followed by a discussion of the optimal (time/fuel) control, with a specific focus on low-Earth-orbit-based satellite clusters. Included in this section are simulations of the maneuvers, as well as a verification of their optimality. The next section addresses cluster optimality, collision avoidance, and noncircular orbits. Finally, the full planner methodology is integrated into a realistic example with $J_2$ and eccentricity effects.

## II. Planner Methodology

Satellite cluster-based planning and control is intimately connected with a thorough understanding of the orbital dynamics. Consider a set of $n$ satellites each with dynamics described as

$$\dot{\boldsymbol{x}}_i = f_i(\boldsymbol{x}_i, \boldsymbol{w}_i, \boldsymbol{u}_i), \qquad i = 1, \ldots, n \tag{1}$$

where $\boldsymbol{x}_i$ is a six-element state vector of positions and velocities in a given coordinate system, $\boldsymbol{w}_i$ is a set of disturbances such as drag and other planetary bodies, and $\boldsymbol{u}_i$ is a thrust input used to control the position within the orbit and/or given coordinate system. To minimize fuel usage, stable solutions are sought to these dynamics, denoted as

$$\boldsymbol{x}_i(t) = s_i(\boldsymbol{\theta}_i, t), \qquad i = 1, \ldots, n \tag{2}$$

where $\theta_i$ is a set of parameters used to describe the stable orbit for the $i$th satellite. Note that the solutions could also be dependent on a variable other than time, such as the true anomaly. These solutions are referred to as a formation in the literature.

If such solutions can be found, the planning and control problem becomes one of two modes of operation: 1) reconfigure from one stable solution $[s_i(\theta_{i,1}, t_1)]$ to the next $[s_i(\theta_{i,2}, t_2)]$ and 2) maintain a satellite within a given stable solution $s_i(\theta_i, t)$ in the presence of disturbances and other nonidealities. The simplest form of relative dynamics and solution is using a reference coordinate frame on a rotating circular orbit. For this case, assuming the size of the cluster is very small compared to orbital radius, the dynamics are very nearly linear. These are the well known Hill's equations (see Ref. 17). Linearizing the Keplerian orbital dynamics about a circular reference orbit yields

$$\begin{aligned} \ddot{x}_i &= 3\omega_n^2 x_i + 2\omega_n \dot{y}_i + w_x + u_x \\ \ddot{y}_i &= -2\omega_n \dot{x}_i + w_y + u_y \\ \ddot{z}_i &= -\omega_n^2 z_i + w_z + u_z \end{aligned} \tag{3}$$

where $x_i$, $y_i$, and $z_i$ are the relative distance from the satellite to the center of an orbiting coordinate frame in the radial, velocity, and cross-track directions, $\omega_n$ is the reference orbital frequency, $w_{(\cdot)}$ are the relative disturbance accelerations, and $u_{(\cdot)}$ are the relative thrust accelerations.

The stable orbit [as defined by Eq. (2)] is simply the homogenous solution of Eq. (3) ($w_{(\cdot)} = u_{(\cdot)} = 0$) and can be written as a $2 \times 1$ planar ellipse in the radial-along-track ($X$–$Y$) plane,[17] or

$$\begin{aligned} x_i(t) &= (R_i/2)\cos(\omega_n t + \alpha_i) \\ y_i(t) &= -R_i \sin(\omega_n t + \alpha_i) \\ z_i(t) &= R_{zi} \cos(\omega_n t + \alpha_{zi}) \end{aligned} \tag{4}$$

where $R_i$ is the ellipse semimajor axis, $\alpha_i$ is the phasing angle of the satellite within the formation ellipse, and $z$ refers to the cross-track axis. Subsequent discussion refers to the $X$–$Y$ axis as the in-plane dynamics because they are in the plane of the reference orbit. Note that the cross-track motion is decoupled.

The parameter vector that defines each stable formation for the circular orbit case is then given as

$$\boldsymbol{\theta}_i = [R_i \quad \alpha_i \quad R_{zi} \quad \alpha_{zi}]^T \tag{5}$$

The parameter vector can be reduced to three elements for some applications, such as defining the in-plane ellipse [the first two parameters of Eq. (5)] and its tilt, which is important for space-based radar.[20] Cluster planning for a reconfiguration, a standard maneuver, is to change from one parameter vector to the next [from $s(\boldsymbol{\theta}_{i,1}, t_1)$ to $s(\boldsymbol{\theta}_{i,2}, t_2)$] in an optimal sense, while avoiding collisions and maintaining science constraints such as timing.

Relative satellite dynamics based on a circular reference orbit have well-known limitations, including the lack of Earth oblateness effects, or $J_2$, and difficulties with noncircular orbits. This causes the planning and control to work more, that is, use more fuel, to maintain and reconfigure the cluster. Schaub and Alfriend[21] recently have defined stable formations that are invariant to $J_2$ effects, whereas Lawden[22] and more recently Inalhan et al.[9] have defined stable formations based on eccentric orbits. The latter is considered here in more detail. The vector $\boldsymbol{\theta}_i$ defining stable formations for eccentric orbits can include more than three parameters because the local movements are no longer simple ellipses in the local frame. However, if only solutions that are symmetric about the local vertical axis are considered, these stable formations can be written in a manner analogous to the circular orbit case,

$$x_i[\nu(t)] = (R_i/2)\cos[\nu(t) + \alpha_i]$$

$$y_i[\nu(t)] = R_i \frac{1 + (e/2)\cos[\nu(t) + \alpha_i]}{1 + e\cos[\nu(t) + \alpha_i]} \sin[\nu(t) + \alpha_i]$$

$$z_i[\nu(t)] = R_{zi} \frac{1}{1 + e\cos[\nu(t) + \alpha_{zi}]} \cos[\nu(t) + \alpha_{zi}] \qquad (6)$$

where $e$ and $\nu(t)$ are the eccentricity and true anomaly of the reference orbit. The phase $\alpha_i$ is now a delay in the true anomaly $\nu(t)$. In this case, the formation is defined using four parameters, as in Eq. (5).

Cluster planning, as defined here, is split into two important steps, as shown in Fig. 1: a fleet planner that considers fuel, time, collisions, and other constraints across the cluster, and a spacecraft planner that considers the specific maneuver plan for each individual satellite within the cluster constraints. In general, at least part of the fleet planner must be implemented in one location, that is, on one satellite or even on the ground, whereas the spacecraft planners can be distributed. The planner methodology considered here uses formations based on the circular reference orbit to define an initial set of control switch times for each satellite. These switch times are then used as an initial guess to an optimization based on more complex dynamics and formations (such as those defined with $J_2$ and $e > 0$) to find the final maneuver switch times. Only a cluster reconfiguration [from $s(\boldsymbol{\theta}_{i,1}, t_1)$ to $s(\boldsymbol{\theta}_{i,2}, t_2)$] is considered here; however, a more general feedforward control methodology is a straightforward extension.

The proposed planner assumes only that a set of parameter vectors for $n$ satellites in the final stable orbit as well as the time constraints are known: $s(\boldsymbol{\theta}_{i,F}, t_F)$ for all $i$. The individual satellite assignments, as well as their specific maneuvers, are not known. In general, this is a difficult problem to solve in an optimal sense, especially as the number of satellites increases. The approach here is based on a two-tiered methodology: satellite assignment and final maneuver generation and is broken down as follows.

### A. Satellite Assignment (SA)

1) Minimum-time/fuel maneuvers are generated for each satellite to all (or a discretized set of) final satellite locations. This is accomplished by solving the optimal control problem for the control switch times.

2) Proximity to collision is calculated by evaluating the minimum distance between each pair of (uncertain) satellite locations during their respective maneuvers.

3) If required, a set of collision avoidance maneuvers is generated by using a variety of start and end times for each maneuver. Thus, each maneuver is still optimal.

4) Final position assignments are evaluated based on minimizing a fuel/proximity-based cost metric with constraints on time and collisions.

### B. Final Maneuver Generation (FG)

1) Final position assignments, maneuver switch times, and collision proximity requirements are delivered to each satellite.

2) Based on the switch times from the chosen maneuver, a final maneuver is generated using more complex models with $J_2$ and eccentricity effects.

3) Each individual satellite can replan to optimize other local parameters such that time and collision constraints are not violated.

The planner methodology considered here attempts to address directly each important requirement within the planning and control paradigm for future satellite clusters. The optimal (fuel/time) control switch times for each satellite maneuver consider control inputs that are compatible with state-of-the-art electric propulsion constraints. Reliable collision avoidance is accomplished by using a variety of start and end times for each maneuver (such as delaying the start of a maneuver to avoid a collision); thus, each maneuver is still time or fuel optimal. Final assignments are distributed using minimal communication of location, collision proximity requirements, and control switch time information. Each individual satellite optimizes its own control input based on realistic, higher fidelity models, thus distributing computation. The optimized maneuver for each satellite is constrained to fall within a particular error ellipse from the original trajectory, thus guaranteeing collision avoidance for the final maneuver.

Note that all steps except for SA 2–4 can be generated by the individual satellites. Thus, as the number of satellites increases, this algorithm scales quite well.

## III. Single-Satellite, Optimal Maneuvers within a Cluster

Relative satellite dynamics, as defined with a circular reference orbit, are convenient to work with because the cross-track motion $Z$ decouples from the in-plane motion $X$ and $Y$. (Note that this also occurs with eccentric orbits.[22]) Converting Eq. (3) to state space (and dropping the $i$ notation for clarity) yields

$$\dot{\boldsymbol{x}} = A\boldsymbol{x} + B\boldsymbol{u} + B_w\boldsymbol{w} \qquad (7)$$

where $\boldsymbol{x} \in \mathbb{R}^6$, $\boldsymbol{u} < U$, and $\boldsymbol{w} \in \mathbb{R}^3$ are the state, input, and disturbance vectors,

$$A = \begin{bmatrix} 0 & 1 & 0 & 0 & 0 & 0 \\ 3\omega_n^2 & 0 & 0 & 2\omega_n & 0 & 0 \\ 0 & 0 & 0 & 1 & 0 & 0 \\ 0 & -2\omega_n & 0 & 0 & 0 & 0 \\ 0 & 0 & 0 & 0 & 0 & 1 \\ 0 & 0 & 0 & 0 & -\omega_n^2 & 0 \end{bmatrix}$$

$$B = B_w = \begin{bmatrix} 0 & 0 & 0 \\ 1/m & 0 & 0 \\ 0 & 0 & 0 \\ 0 & 1/m & 0 \\ 0 & 0 & 0 \\ 0 & 0 & 1/m \end{bmatrix}$$

$$\boldsymbol{x} = [x \quad \dot{x} \quad y \quad \dot{y} \quad z \quad \dot{z}]^T, \qquad \boldsymbol{u} = [u_x \quad u_y \quad u_z]^T$$

$$\boldsymbol{w} = [w_x \quad w_y \quad w_z]^T$$

Small thrust, electric propulsion is assumed; therefore, the mass is assumed to be constant. This implies that the optimal control problem can be decoupled as well. The cross-track motion can be modeled as a simple spring–mass oscillator, whereas the in-plane system consists of a rigid-body mode and one oscillatory

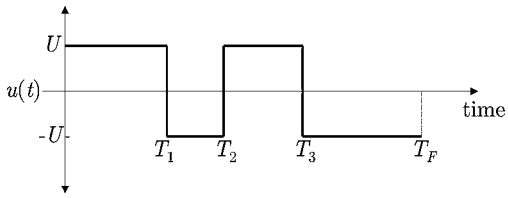


**a) Minimum-time maneuver**

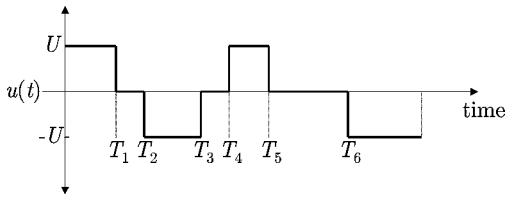


**b) Minimum-fuel maneuver**

**Fig. 2 Assumed switching functions for in-plane ($X$–$Y$) minimum-time and minimum-fuel maneuvers.**

mode. Minimum-time/fuel maneuvers for simple oscillators are well known.[23] Because of this, the in-plane problem is discussed in detail here, whereas the results of the simpler two-state system of the cross-track dynamics are presented for completeness, with little discussion. Also, in the development, only thrust in the $Y$ and $Z$ directions is considered because they are the most common.

Defining a true time/fuel optimal control input is usually difficult for all but the simplest cases. Many times, assuming an intuitive form of the control input and testing optimality in trial-and-error fashion works well. It is well known that the minimum-time solution is bang–bang.[24] It follows that the form of the minimum-time control for the in-plane $X$–$Y$ system is shown in Fig. 2a for maneuvers that are less than one orbit in length. This is intuitively correct because it is well known that, for stable $n$-state systems, the number of required switch times is $n-1$ (Ref. 24). There are four unknowns, including the three switching times $T_i$ and the final time $T_F$. The switching times $T_i$ considered here are in normalized time, or $T_i = \omega_n(t_i - t_0)$. For the two-state, cross-track system, there is one switch time $T_{z1}$ and a different final time $T_{zF}$.

The minimum-fuel maneuver for the four-state, in-plane problem is similar, as shown in Fig. 2b. In this case, after each constant thrust input is applied, there is a period where the satellite "coasts" to the next switching point. There are six unknowns, which include the six switching times $T_i$; the final time is given. These assumed switching input functions are used to find the time- and fuel-optimal control maneuvers; they are also verified to be the optimal solutions in the examples presented.

### A. Minimum-Time Maneuvers

Minimum time maneuvers are characterized by Pontryagin's maximum principle (see Ref. 24) with a cost defined as

$$J_{\text{time}} = \int_{t_0}^{t_F} \mathrm{d}t \tag{8}$$

Using this cost function, the Hamiltonian can be defined as

$$\mathcal{H}_{\text{time}}(t) = 1 + \boldsymbol{p}^T(t)[A\boldsymbol{x}(t) + B\boldsymbol{u}(t)] \tag{9}$$

where $\boldsymbol{p}(t)$ is the costate and is defined as

$$\dot{\boldsymbol{p}} = -A^T\boldsymbol{p}(t) \tag{10}$$

The initial and final state conditions for the maneuver are written as

$$\boldsymbol{x}_0 = \begin{bmatrix} x_0 \\ y_0 \\ z_0 \end{bmatrix} = \begin{bmatrix} (R_0/2)\cos(\alpha_0) \\ -R_0\sin(\alpha_0) \\ R_{z0}\sin(\alpha_{z0}) \end{bmatrix} \tag{11}$$

$$\boldsymbol{x}_F = \begin{bmatrix} x_F \\ y_F \\ z_F \end{bmatrix} = \begin{bmatrix} (R_F/2)\cos(T_F + \alpha_F) \\ -R_F\sin(T_F + \alpha_F) \\ R_{zF}\sin(T_F + \alpha_{zF}) \end{bmatrix} \tag{12}$$

where 0 and $F$ refer to initial and final, respectively. When the in-plane $X$–$Y$, four-state problem is considered first (the system matrices, state vector, etc., are shortened appropriately), and the maneuver defined in Fig. 2a, the state can be propagated forward in time. The time-optimal constraint equations can then be written as

$$\boldsymbol{x}_F = \exp\left[A\left(\frac{T_F}{\omega_n}\right)\right]\boldsymbol{x}_0 + \int_0^{T_F/\omega_n} \exp\left[A\left(\frac{T_F}{\omega_n} - \tau\right)\right]B\boldsymbol{u}(\tau)\,\mathrm{d}\tau \tag{13}$$

$$\boldsymbol{p}^T(T_i)B = 0, \qquad \forall\, T_i \tag{14}$$

There is also an additional constraint equation on the Hamiltonian for minimum-time commands, which is

$$\mathcal{H}_{\text{time}}(t) = 0, \qquad \forall t \tag{15}$$

For the four-state system, Eq. (13) yields four constraints [simplified in Eq. (16)], Eq. (14) yields three constraints, and Eq. (15) yields one constraint [both simplified in Eq. (17)] for a total of $4+3+1=8$ constraints. These eight constraint equations can be used to solve for the eight unknowns: three switching times $T_1 - T_3$, the final time $T_F$, and four initial conditions on the costate, $p_1 - p_4$. Note that the cross-axis constraints [Eqs. (18) and (19)] are shown for completeness.

$$\begin{aligned} &T_F^2/2 - T_1^2 + T_2^2 - T_3^2 = 0, \qquad T_F/2 - T_1 + T_2 - T_3 = 0 \\ &c_0\sin(\alpha_0) - \cos(T_1) + \cos(T_2) - \cos(T_3) \\ &\quad + [1 + \cos(T_F)]/2 - c_F\sin(\alpha_F) = 0 \\ &c_0\cos(\alpha_0) - \sin(T_1) + \sin(T_2) - \sin(T_3) \\ &\quad + \sin(T_F)/2 - c_F\cos(\alpha_F) = 0 \end{aligned} \tag{16}$$

$$\begin{bmatrix} 2\cos(T_1)-2 & 2\sin(T_1) & 4\sin(T_1)-3T_1 & 3-4\cos(T_1) \\ 2\cos(T_2)-2 & 2\sin(T_2) & 4\sin(T_2)-3T_2 & 3-4\cos(T_2) \\ 2\cos(T_3)-2 & 2\sin(T_3) & 4\sin(T_3)-3T_3 & 3-4\cos(T_3) \\ \frac{R_0}{2}\sin(\alpha_0) & \frac{R_0}{2}\cos(\alpha_0) & R_0\cos(\alpha_0) & -R_0\sin(\alpha_0) - \frac{U}{\omega_n^2 m} \end{bmatrix} \times \begin{bmatrix} p_1 \\ \omega_n \cdot p_2 \\ p_3 \\ \omega_n \cdot p_4 \end{bmatrix} = \begin{bmatrix} 0 \\ 0 \\ 0 \\ \dfrac{1}{\omega_n} \end{bmatrix} \tag{17}$$

$$\begin{aligned} &c_{z0}\cos(\alpha_{z0}) + \cos(T_{z1}) - [\cos(T_{zF}) + 1]/2 - c_{zF}\cos(\alpha_{zF}) = 0 \\ &-c_{z0}\sin(\alpha_{z0}) + \sin(T_{z1}) - [\sin(T_{zF})/2] + c_{zF}\sin(\alpha_{zF}) = 0 \end{aligned} \tag{18}$$

$$\begin{bmatrix} \sin(T_{z1}) & -\cos(T_{z1}) \\ R_{z0}\sin(\alpha_{z0}) & R_{z0}\cos(\alpha_{z0}) - U_z/m\omega_n^2 \end{bmatrix} \begin{bmatrix} p_{z1} \\ \omega_n \cdot p_{z2} \end{bmatrix} = \begin{bmatrix} 0 \\ 1/\omega_n \end{bmatrix} \tag{19}$$

where

$$c_0 = \frac{R_0\omega_n^2 m}{8U}, \qquad c_F = \frac{R_F\omega_n^2 m}{8U}, \qquad c_{z0} = \frac{R_{z0}\omega_n^2 m}{U}$$

$$c_{zF} = \frac{R_{zF}\omega_n^2 m}{U}, \qquad T_{(\cdot)} = \omega_n(t_{(\cdot)} - t_0)$$

and $z$ refers to the cross-axis dynamics. The switch times, final time, and costate initial conditions are then solved using a numerical technique. In the cases presented here, a computationally reliable gradient search technique in MATLAB® is used. An initial guess spaced equally for a one orbit maneuver allowed the solution to converge quickly and reliably.

The solution to the single satellite, minimum-time maneuver problem within a cluster is similar to the rigid-body/flexible-mode slewing problem presented in Refs. 25 and 26. Thus, all optimality proofs can be applied here as well. The cases presented here do not have as many flexible modes, but have more complex initial and final conditions. Once all constraint equations have been satisfied, optimality can be verified using Eqs. (9) and (15).

As an example, consider the following maneuver for one satellite, changing both its in-plane ellipse size and phasing:

$$\boldsymbol{\theta}_0 = \begin{bmatrix} 250\text{ m} \\ 0\text{ deg} \\ 0\text{ m} \\ 0\text{ deg} \end{bmatrix} \longrightarrow \boldsymbol{\theta}_F = \begin{bmatrix} 300\text{ m} \\ -22\text{ deg} \\ 0\text{ m} \\ 0\text{ deg} \end{bmatrix} \tag{20}$$

When the minimum-time constraints are solved in Eq. (16), the three switching times and final time are (in units of orbits):

$$[T_1, T_2, T_3, T_F] = [0.000, 0.106, 0.316, 0.421] \tag{21}$$

This implies that there are only two switching times, not three; the significance of this design is discussed later in the cluster planner section. Once the switching times and final time are known, the initial costate vector can be found using Eq. (17). It then follows that the switching conditions [Eq. (14)] and optimality [Eqs. (9) and (15)] can be checked to verify that the solution is optimal.

Figure 3a shows the scaled input $u(t)/U$, as well as the switching function $\boldsymbol{p}^T(t)B$. Each of the switching constraints, given as $\boldsymbol{p}^T(T_i)B = 0$, are met for all three switching times, including $T_1 = 0$. Figure 3 shows a plot of the Hamiltonian, which is within $\pm 0.0002$ of the desired value of $\mathcal{H}_{\text{time}}(t) = 0$. Figure 4 shows the initial and final stable formation ellipses, as well as the maneuver, in the $X$–$Y$ plane.

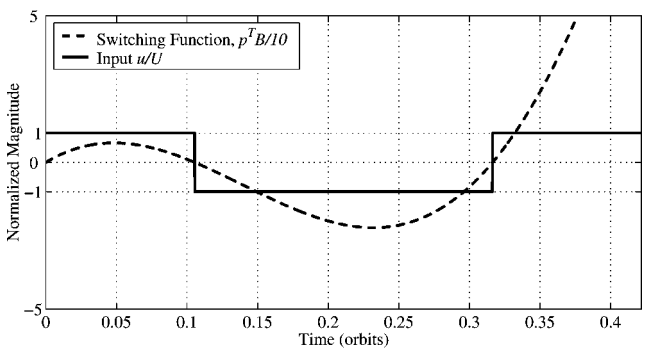


a)

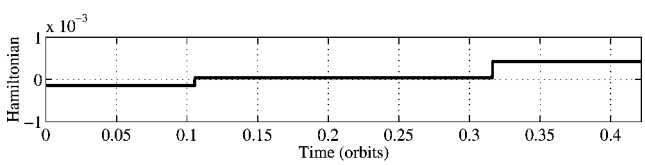


b)

**Fig. 3 Minimum time, in-plane ($X$–$Y$) maneuver from $R_0$ = 250 m, $\alpha_0$ = 0 deg to $R_F$ = 300 m, $\alpha_F$ = −22 deg.**

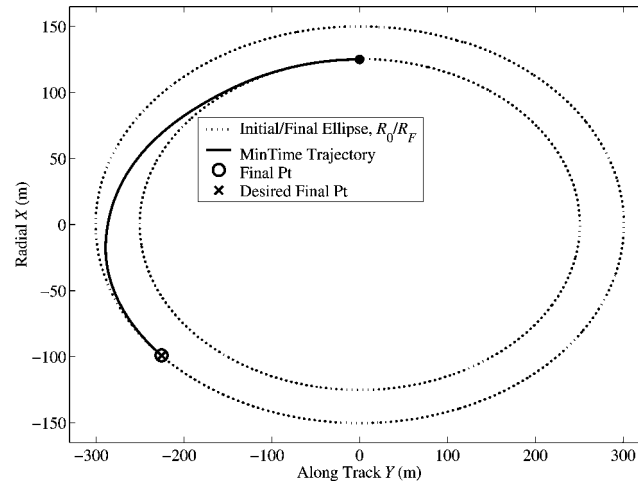


**Fig. 4 Trajectory for the minimum-time maneuver in the $X$–$Y$ plane, along with the initial and final stable formation ellipses.**

As shown, the maneuver starts and ends at the correct conditions. Note that the maneuver takes approximately $T_F = 0.421$ orbits to complete.

### B. Minimum-Fuel Maneuvers

Minimum-fuel maneuvers are found in a similar manner, but are more complicated because there are now six unknown switching times for the in-plane problem. The minimum-fuel cost is given as

$$J_{\text{fuel}} = \int_0^{t_F} |\boldsymbol{u}(t)|\,\mathrm{d}t \tag{22}$$

Using this cost function, the Hamiltonian can be defined as

$$\mathcal{H}_{\text{fuel}}(t) = |\boldsymbol{u}(t)| + \boldsymbol{p}^T(t)[A\boldsymbol{x}(t) + B\boldsymbol{u}(t)] \tag{23}$$

The state, costate, and initial/final conditions are identical to those in the minimum-time problem [Eqs. (10–12)]. When the maneuver defined in Fig. 2b and the initial/final conditions defined in Eqs. (11) and (12) are used, a set of constraint equations can be developed:

$$\boldsymbol{x}_F = \exp\left[A\left(\frac{T_F}{\omega_n}\right)\right]\boldsymbol{x}_0 + \int_0^{T_F/\omega_n} \exp\left[A\left(\frac{T_F}{\omega_n} - \tau\right)\right]B\boldsymbol{u}(\tau)\,\mathrm{d}\tau \tag{24}$$

$$\boldsymbol{p}^T(T_i)B = \operatorname{sgn}(U), \qquad \forall\, T_i \tag{25}$$

The costate constraints imply that

$$U(t)\begin{cases} = +U & \text{if} \quad \boldsymbol{p}^T(t)B < -U \\ = 0 & \text{if} \quad -U \geq \boldsymbol{p}^T(t)B \geq +U \\ = -U & \text{if} \quad \boldsymbol{p}^T(t)B > +U \end{cases} \tag{26}$$

For the four state system, Eqs. (24) and (25) yield $4 + 6 = 10$ constraints, which can be used to solve for the 10 unknowns: 6 switching times $T_1 - T_6$ and 4 initial conditions on the costate, $p_1 - p_4$. The Hamiltonian, which is again used as a verification, is defined as a constant over all time,

$$\mathcal{H}_{\text{fuel}}(t) = \text{const}, \qquad \forall\, t \tag{27}$$

The constraint equations can be simplified to those shown in Eqs. (28–31); the cross-axis constraints are shown for completeness. A complicating feature of the minimum-fuel constraint equations is that they are now coupled.

$$-T_1^2 - T_2^2 + T_3^2 + T_4^2 - T_5^2 - T_6^2 + T_F^2 = 0$$

$$-T_1 - T_2 + T_3 + T_4 - T_5 - T_6 + T_F = 0$$

$$-c_0 \sin(\alpha_0) - \cos(T_1) - \cos(T_2) + \cos(T_3) + \cos(T_4) - \cos(T_5) - \cos(T_6) + \cos(T_F) + c_F \sin(\alpha_F) + 1 = 0$$

$$-c_0 \cos(\alpha_0) - \sin(T_1) - \sin(T_2) + \sin(T_3) + \sin(T_4) - \sin(T_5) - \sin(T_6) + \sin(T_F) + c_F \cos(\alpha_F) = 0 \tag{28}$$

$$\begin{bmatrix} 2\cos(T_1) - 2 & 2\sin(T_1) & -3T_1 + 4\sin(T_1) & 3 - 4\cos(T_1) \\ 2\cos(T_2) - 2 & 2\sin(T_2) & -3T_2 + 4\sin(T_2) & 3 - 4\cos(T_2) \\ 2\cos(T_3) - 2 & 2\sin(T_3) & -3T_3 + 4\sin(T_3) & 3 - 4\cos(T_3) \\ 2\cos(T_4) - 2 & 2\sin(T_4) & -3T_4 + 4\sin(T_4) & 3 - 4\cos(T_4) \\ 2\cos(T_5) - 2 & 2\sin(T_5) & -3T_5 + 4\sin(T_5) & 3 - 4\cos(T_5) \\ 2\cos(T_6) - 2 & 2\sin(T_6) & -3T_6 + 4\sin(T_6) & 3 - 4\cos(T_6) \end{bmatrix}$$

$$\times \begin{bmatrix} p_1 \\ \omega_n \cdot p_2 \\ p_3 \\ \omega_n \cdot p_4 \end{bmatrix} = \begin{bmatrix} +1 \\ -1 \\ -1 \\ +1 \\ +1 \\ -1 \end{bmatrix} \operatorname{sgn}(U) m \omega_n \tag{29}$$

$$-8c_{z0} \sin(\alpha_{z0}) + \sin(T_{z1}) + \sin(T_{z2}) - \sin(T_{zF}) + 8c_{zF} \sin(\alpha_{zF}) = 0$$

$$-8c_{z0} \cos(\alpha_{z0}) + \cos(T_{z1}) - 1 + \cos(T_{z2}) - \cos(T_F) - 8c_{zF} \cos(\alpha_{zF}) = 0 \tag{30}$$

$$\begin{bmatrix} \sin(T_{z1}) & -\cos(T_{z1}) \\ \sin(T_{z2}) & -\cos(T_{z2}) \end{bmatrix} \begin{bmatrix} p_{z1} \\ \omega_n \cdot p_{z2} \end{bmatrix} = \begin{bmatrix} +1 \\ -1 \end{bmatrix} \operatorname{sgn}(U_z) m \omega_n \tag{31}$$

where

$$c_0 = \frac{R_0 \omega_n^2 m}{4U}, \qquad c_F = \frac{R_F \omega_n^2 m}{4U}, \qquad c_{z0} = \frac{R_{z0} \omega_n^2 m}{U}$$

$$c_{zF} = \frac{R_{zF} \omega_n^2 m}{U}, \qquad T_{(\cdot)} = \omega_n (t_{(\cdot)} - t_0)$$

As an example, consider the same maneuver as in the preceding section, described in Eq. (20), but now a final time of $T_F = 0.9$ orbits is specified. This final time implies that the satellite cluster requires reconfiguration before returning to a similar point over the Earth after one orbit. Solving the minimum-fuel constraints in Eq. (28) and the first two entries of Eq. (29) for the switching times yields (in units of orbits):

$$[T_1, T_2, T_3, T_4, T_5, T_6] = [0.024, 0.232, 0.285, 0.619, 0.670, 0.878] \tag{32}$$

Once the switching times are known, the initial costate vector can be found from the final four entries of Eq. (29). It then follows that the switching conditions [Eq. (26)] and the Hamiltonian [Eqs. (23) and (27)] can be checked to verify that the solution is optimal.

Figure 5a shows the scaled input $u(t)/U$, as well as the switching function $\boldsymbol{p}^T(t)B$. Each of the switching constraints, given as $\boldsymbol{p}^T(T_i)B = \pm U$, are met for all six switching times. Figure 5 shows

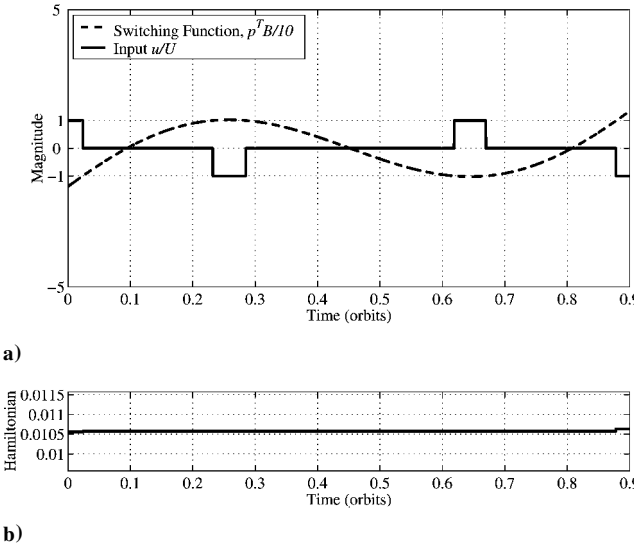


**Fig. 5 Minimum-fuel, in-plane ($X$–$Y$) maneuver from $R_0 = 250$ m, $\alpha_0 = 0$ deg to $R_F = 300$ m, $\alpha_F = -22$ deg; maneuver time $T_F = 0.9$ orbits.**

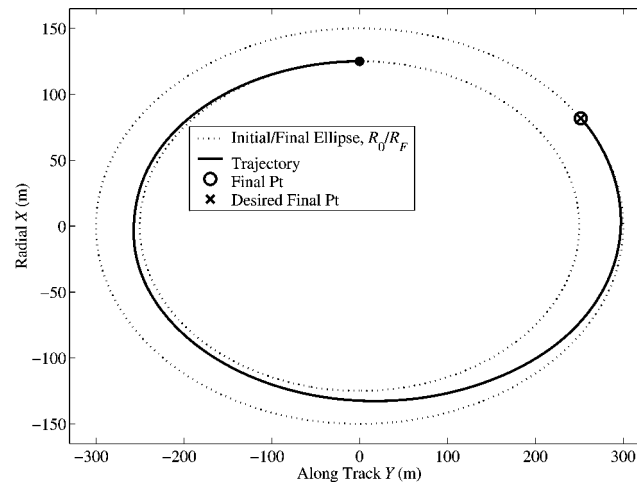


**Fig. 6 Trajectory for minimum-fuel maneuver in $X$–$Y$ plane, along with the initial and final stable formation ellipses.**

the Hamiltonian, which is within $\pm 0.001$ of the desired value of $\mathcal{H}_{\text{fuel}}(t) = 0.106$. Figure 6 shows the initial and final stable formation ellipses, as well as the maneuver, in the $X$–$Y$ plane. As shown, the maneuver starts and ends at the correct conditions.

## IV. Multiple Satellite Planner

Extending the optimal control concept to multiple satellites is a challenging task. The approach here is to use the single-satellite, optimal control developed in the preceding section to search over the remaining cluster parameters quickly to achieve time/fuel optimality at the cluster level. This section addresses three important interrelated concepts: multiple satellite optimal maneuvers, collisions, and noncircular effects.

### A. Multiple-Satellite, Optimal Maneuvers

In multiple-satellite planning and control, the stable formations to be used are driven by the science requirements. As such, there are many different definitions of formations and reconfiguration between formations. Here, a general approach is developed. Given $n$ satellites, a multiple-satellite reconfiguration is defined as a transfer from $n$ locations in a stable formation to $n$ new locations in a stable formation. This can be written as

$$S_0 = \left\{ \begin{bmatrix} R_0 \\ \alpha_0 \\ R_{z0} \\ \alpha_{z0} \end{bmatrix}_1, \ldots, \begin{bmatrix} R_0 \\ \alpha_0 \\ R_{z0} \\ \alpha_{z0} \end{bmatrix}_n \right\} \longrightarrow$$

$$S_F = \left\{ \begin{bmatrix} R_F \\ \alpha_F \\ R_{zF} \\ \alpha_{zF} \end{bmatrix}_1, \ldots, \begin{bmatrix} R_F \\ \alpha_F \\ R_{zF} \\ \alpha_{zF} \end{bmatrix}_n \right\} \tag{33}$$

where $S_{(\cdot)}$ is a set of $n$ locations in a stable formation at a given time. This optimal control problem could be solved by evaluating the optimal trajectory for each satellite from its original position to all final positions and evaluating the cost. Because the optimal control laws can be solved quickly based on the equations of the preceding section, this type of planner is quite simple to implement.

A more complicated reconfiguration is to allow the final phasing to vary and constrain the relative phasing between spacecraft. This is written with a final stable formation as

$$S_F = \left\{ \begin{bmatrix} R_F \\ \alpha_F \\ R_{zF} \\ \alpha_{zF} \end{bmatrix}_1, \begin{bmatrix} R_F \\ \alpha_F + \Delta\alpha_{z,F} \\ R_{zF} \\ \alpha_{zF} + \Delta\alpha_{z,zF} \end{bmatrix}_2, \ldots, \begin{bmatrix} R_F \\ \alpha_F + \Delta\alpha_{n,F} \\ R_{zF} \\ \alpha_{zF} + \Delta\alpha_{n,zF} \end{bmatrix}_n \right\} \tag{34}$$

where $\Delta\alpha_{i,F}$ and $\Delta\alpha_{i,zF}$ are given and $\alpha_F$ and $\alpha_{zF}$ are unknown. Assuming the cluster planner solution is a function only of the in-plane dynamics, the parameter $\alpha_F$ is chosen in order to minimize the time or fuel of the full cluster, rather than that of a single satellite. This leads to concepts such as time/fuel maps as a function of spacecraft phasing $\alpha_F$.

Consider a four-satellite cluster, with the following reconfiguration to be planned:

$$S_0 = \left\{ \begin{bmatrix} 250 & \text{m} \\ (0, 90, 180, -90) & \text{deg} \\ 0 & \text{m} \\ (0, 90, 180, -90) & \text{deg} \end{bmatrix} \right\} \longrightarrow$$

$$S_F = \left\{ \begin{bmatrix} 300 & \text{m} \\ \alpha_F + (0, 90, 180, -90) & \text{deg} \\ 0 & \text{m} \\ (0, 90, 180, -90) & \text{deg} \end{bmatrix} \right\} \tag{35}$$

where the relative phasing between all four satellites is 90 deg and $\alpha_F$ is a parameter to be chosen to minimize the time for the full cluster to complete the reconfiguration.

The final time $T_F$ and initial switch time $T_1$ for one satellite are shown in Fig. 7 for a maneuver from $[\alpha_0]_1 = 0$ deg to a final phasing condition $[\alpha_F]_1 = \alpha_F$ deg with discretization levels of 1 deg in $\alpha_F$. The minimum-time maneuver for this satellite is to a final phasing of $[\alpha_F]_1 = -22$ deg, which corresponds to the maneuver presented in Figs. 3 and 4. Again, note that there are only two switch times for this maneuver and that $T_1 = 0$. The solutions for all 360 optimal maneuvers were generated in 20 s on a Pentium IV, 1.4-GHz machine in MATLAB.

The time map as a function of spacecraft phasing in the final formation can be generated for all four satellites and then combined to evaluate cluster maneuver optimality. Given 1-deg discretization levels in final phasing, there are $360 \times 4 = 1440$ optimal control problems to be solved; this takes $\approx$1 min on a Pentium IV, 1.4-GHz machine in MATLAB. The individual satellite time maps can then be combined into $360 \times 2^4 = 5760$ possible reconfiguration options. This includes all cases, including those where the satellites have "cross" phasing, such as $[\alpha_0]_1 = 0$, $[\alpha_0]_2 = 90$ deg to $[\alpha_F]_1 = \alpha_F + 90$, $[\alpha_F]_2 = \alpha_F + 0$ deg.

For the four-satellite reconfiguration given in Eq. (35), the final time $T_F$ for all four satellites (no crossings) is shown in Fig. 8.

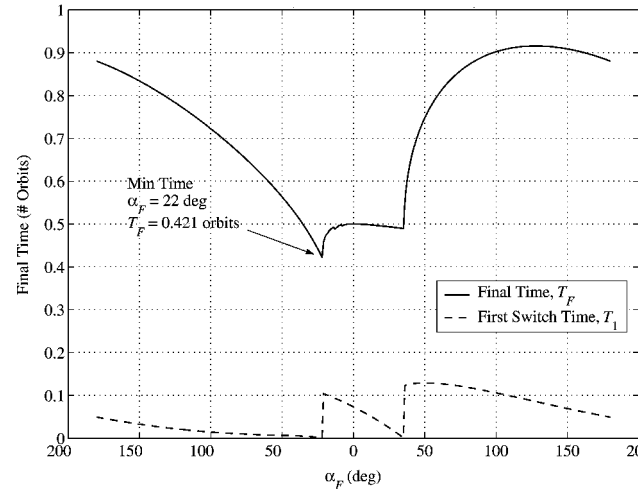


**Fig. 7 Final time $T_F$ and initial switch time $T_1$ for a minimum-time maneuver from $R_0 = 250$ m, $\alpha_0 = 0$ deg to $R_F = 300$ m, $\alpha_F$ deg.**

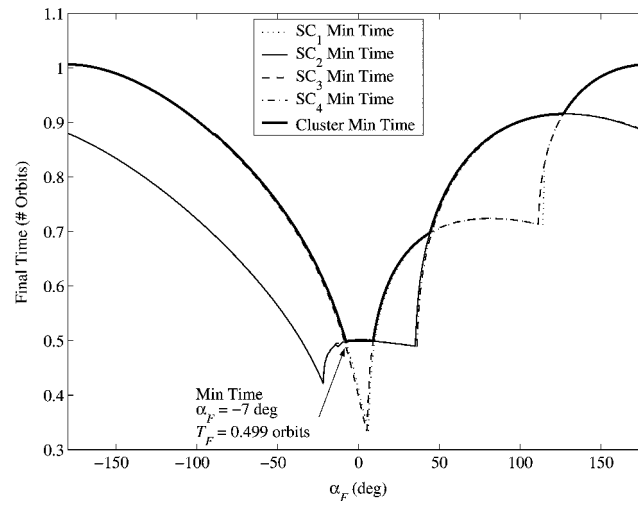


**Fig. 8 Cluster-based minimum-time maneuver from $R_0 = 250$ m, $\alpha_0 = 0$ deg to $R_F = 300$ m, $\alpha_F$ deg for all four satellites; final maneuver time as a function of final phasing parameter.**

Because of the symmetry of the problem, the time maps for individual satellites that start at $[\alpha_0]_1 = 0$, $[\alpha_0]_3 = 180$ deg are identical, as are the maps for $[\alpha_0]_2 = 0$, $[\alpha_0]_4 = 180$. The minimum time for the cluster to reconfigure is then written as

$$T_{\text{mintimecluster}} = \min_{\alpha_F} \max_i \{T_{i,F}\} \tag{36}$$

In this case, the minimum time for cluster reconfiguration is $T_{\text{mintimecluster}} = 0.499$ orbits, which corresponds to spacecraft phasing (in degrees) of

$$[\alpha_F]_1 = -7, \qquad [\alpha_F]_4 = -97$$
$$[\alpha_F]_2 = 83, \qquad [\alpha_F]_3 = 173 \tag{37}$$

Obviously, fuel maps could be developed in an analogous fashion to the time maps just described. As a comparison between minimum-time and minimum-fuel maneuvers, consider Fig. 9, where the fuel usage for both cases is presented for the full complement of final ellipse phasing (again no crossing). The final time for the minimum-fuel cases is $T_F = 0.9$ orbits. Obviously, the minimum-fuel case always uses less fuel. In the $\alpha_F = 97$–$163$ deg region, the minimum-fuel maneuver does not exist because the maneuver cannot be completed in under 0.9 orbits.

The work here forms the basis from which many different types of planners can be generated. For example, the actual selection of

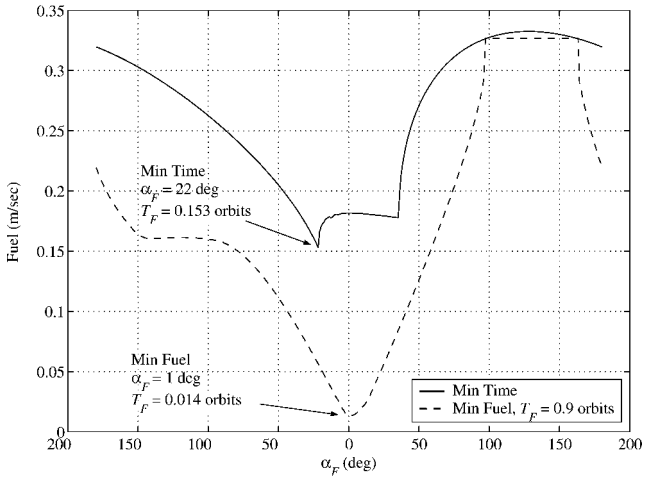


**Fig. 9 Comparison of minimum time and fuel maneuvers for single-satellite maneuver within a cluster, orbit maneuver $R_0$ = 250 m to $R_F$ = 300 m, $\alpha_0$ = 0 deg.**

the final maneuver may also want to take into account past maneuvers and/or current resources such as fuel remaining. This could easily be added to the planner by adjusting the cluster-based cost [Eq. (36)], while using the same time and fuel maps generated in this work. Schetter et al.[10] describe a bidding mechanism that uses these additional factors, based on the minimum-fuel maps developed here.

### B. Collision Avoidance

Adding collision constraints to the minimum-time/fuel optimization problem makes it difficult to find a general assumed form for the maneuver, as in Fig. 2. Here, collision avoidance is addressed by evaluating the collision proximity and, if necessary, using different maneuver start and end times to generate collision avoidance maneuvers. This is intuitively appealing because the maneuvers are still time/fuel optimal, although not necessarily optimal in terms of maneuvering to avoid the collision. This approach is, however, more efficient than attempting a maneuver in midtrajectory to avoid a collision.

The approach to collision evaluation follows the development in Ref. 5. Collision monitoring assumes that the initial state and disturbance are bounded by uncertainty ellipsoids given as

$$[\boldsymbol{x}_i(t_0) - \hat{\boldsymbol{x}}_i(t_0)]^T \Sigma_i(t_0)^{-1} [\boldsymbol{x}_i(t_0) - \hat{\boldsymbol{x}}_i(t_0)] \leq 1 \tag{38}$$

$$\boldsymbol{w}_i(t)^T Q_i(t)^{-1} \boldsymbol{w}_i(t) \leq 1 \tag{39}$$

where $\boldsymbol{x}_i(t_0)$ is the initial state, $\hat{\boldsymbol{x}}_i(t_0)$ is the center of the uncertainty ellipsoid set for the $i$th satellite, and the matrices $\Sigma_i(t_0)$, and $Q_i(t)$ are symmetric and positive definite. The definition of the disturbance using an ellipsoid allows for very general exogenous signals, including bias and random types. This is important for relative satellite dynamics because the disturbances are non-Gaussian. For example, differential drag results in a chi-square-like distribution.

These initial ellipsoid sets, based usually on a level of probability desired, are then propagated forward in time to find the reachable space for each individual satellite; this space is used to calculate collision proximity. When the control input $\boldsymbol{u}_i(t)$ is assumed known, the evolution of the initial ellipsoid set in the presence of a disturbance $\boldsymbol{w}_i(t)$ is

$$\hat{\boldsymbol{x}}_i(t) = \exp[A(t-t_0)]\,\hat{\boldsymbol{x}}_i(t_0) + \int_{t_0}^{t} \exp[A(t-\tau)] B \boldsymbol{u}_i(\tau)\,\mathrm{d}\tau \tag{40}$$

$$\Sigma_i(t) = \frac{\{\exp[A(t-t_0)]\}\Sigma_i(t_0)\{\exp[A(t-t_0)]\}^T}{1-\beta} + \frac{\bar{B}_{wi}\bar{B}_{wi}^T}{\beta} \tag{41}$$

where

$$\bar{B}_{wi} = \int_{t_0}^{t} \exp[A(t-\tau)] B_w Q_i(\tau)^{\frac{1}{2}}\,\mathrm{d}\tau$$

and $\beta$ is an optimization parameter that lies between 0 and 1 and is used to minimize the volume or similar metric of the output ellipsoid. The $\beta$ parameter is necessary because the addition of two ellipsoids has no closed-form solution and must be bounded; Ref. 27 yields a closed-form solution for minimizing the trace of the bounding ellipsoid. Equations (40) and (41) yield the center and an ellipsoid bound propagated forward in time $t$ for one satellite,

$$[\boldsymbol{x}_i(t) - \hat{\boldsymbol{x}}_i(t)]^T \Sigma_i(t)^{-1} [\boldsymbol{x}_i(t) - \hat{\boldsymbol{x}}_i(t)] \leq 1 \tag{42}$$

Note that Eqs. (40) and (41) are analogous to the prediction step of the Kalman filter, with the addition of the parameter $\beta$, which is used to conservatively bound the addition of non-Gaussian signals.

Once a maneuver map has been generated, as in Fig. 8, the collision proximity can be evaluated for a smaller subset of the maneuvers. When the minimum-time example in Fig. 8 is considered, collision proximity may be calculated for phasings about the optimum (−7 deg), or $\alpha_F = -20$ to +15 deg. Collision proximity is then calculated for each satellite "pair." Collision proximity is defined as the minimum distance between two uncertainty ellipsoids [$\hat{x}_i(t)$ and $\Sigma_i(t)$]. Because the control inputs are constant over time, the collision proximity for each pair can be calculated very quickly.

If a collision falls within an acceptable proximity range, then a new maneuver must be generated. The approach here is to vary the maneuver start and finish times to generate a new set of maneuvers that will avoid the collision. Consider a new set of initial and final time conditions:

$$[t_0]_{\text{new}} = t_0 \pm \Delta t_0, \qquad [t_F]_{\text{new}} = t_F \pm \Delta t_F \tag{43}$$

A subset of these may also be used; for instance, science requirements may dictate that $+\Delta t_F$ is not allowable. These new times can be integrated into the constraint equations either by defining 1) a new time reference $T_i$, $T_F$ or 2) a new phasing. The new phasing can be written as

$$[\alpha_0]_{\text{new}} = \alpha_0 \pm \omega_n \Delta t_0, \qquad [\alpha_F]_{\text{new}} = \alpha_F \pm \omega_n \Delta t_F \tag{44}$$

As an example, consider the fuel-optimal case shown in Fig. 10. Here, base maneuvers for two satellites, as well as a new collision avoidance maneuver, are compared. Figure 10a and 10b show the original maneuver, as well as the new collision avoidance (CA) maneuver. The latter is generated by shortening the total maneuver time by 2 min (which is equivalent to approximately 7 deg in sweep angle) and also increases fuel usage by 2%. Figure 10c shows the relative separation distance between the satellites (with their uncertainties) as a function of time. As is shown, the proximity between the satellites increases by 5% using this new CA maneuver.

In general, it has been noted during simulations that when the satellites do not switch relative phasings within the cluster, that is, cross, during the maneuver, collisions are not likely except in the cases of very tight clusters. This allows the individual satellites themselves to have more freedom in their maneuver generation (such as considering power/communication/ computation optimal maneuvers), while still maintaining collision constraints.

To address this situation, the evolving uncertainty ellipsoids are scaled in size to an acceptable level of collision proximity. Consider the uncertainty ellipsoid written as

$$\Sigma_i(t) = \frac{\{\exp[A(t-t_0)]\}\Sigma_i(t_0)\{\exp[A(t-t_0)]\}^T}{1-\beta} + \sigma_{\text{ca}} \frac{\bar{B}_{wi}\bar{B}_{wi}^T}{\beta} \tag{45}$$

where the parameter $\sigma_{\text{ca}}$ is a scaling parameter with a nominal value of one used to give a measure of control each individual satellite can add to change its own trajectory while still avoiding collisions. Note for the case shown in Fig. 10, $\sigma_{\text{ca}} = 1$ implies that the collision proximity is 161 m. The parameter $\sigma_{\text{ca}}$ can be increased for each

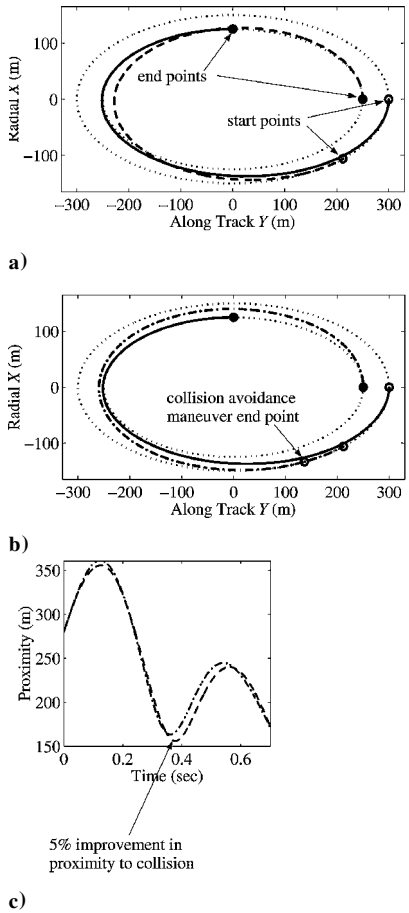


**Fig. 10 Example of CA between two satellites during reconfiguration; the avoidance maneuver utilizes a shortened (by 2 min) maneuver time: ···, initial/final cluster ellipses; ——, minimum-fuel trajectory spacecraft 1; – – –, minimum-fuel trajectory spacecraft 2; and ·–·–, delayed minimum-fuel trajectory.**

satellite until the collision proximity is within acceptable levels. For instance, if an acceptable level of collision proximity is 50 m, the scaling value for the case shown in Fig. 10 is $\sigma_{ca} = 28$. This creates a reachable ellipsoidal "tube" within which each satellite can generate slightly different maneuvers and still avoid collisions. Obviously, other constraints, such as time, must still be maintained.

### C. $J_2$ and Eccentricity Effects

As discussed at the start of this paper, it is important to utilize very accurate, stable solutions to the orbital dynamics to minimize-fuel usage. Recent work has addressed cases including $J_2$ (Ref. 21) and eccentricity[19] effects. In both, although the dynamics are complex, state transitions can be found. Because of this, the theory developed in this work (the constraint equations, as well as the collision proximity evaluation) can be adapted based on the new set of dynamics. In addition, using stable formations for these cases, the switching times developed in this work can be used as initial conditions for optimization to linear time varying or nonlinear dynamics.

Consider the case of varying eccentricity, and use the switching times for the second satellite in Eq. (35), $[\alpha_F]_2 = 90$ deg. Here, a Keplerian model that includes $J_2$ and eccentricity effects is used. The switching times from the circular orbit case are used as an initial guess to an optimization on a Keplerian model. The eccentric stable formations are defined using Eq. (6). Figure 11 shows the switching times as a function of the eccentricity. (The $J_2$ effects are minimal for such a short maneuver.) The switching times change slightly, although not as much as intuition may allow. This allows the theory developed in this paper to be quite practical for cases with more complex dynamics. Based on many simulations, the approach appears to converge reliably for $e < 0.2$; for eccentricities larger than

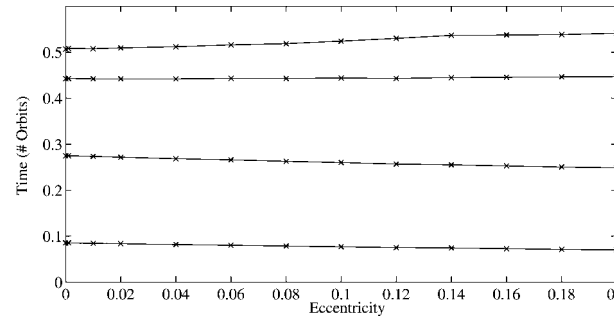


**Fig. 11 Minimum-time switch times and final time as a function of eccentricity, based on optimization using Keplerian model that includes $J_2$ and eccentricity effects.**

this, the theory developed in this paper can be applied to dynamics relative to general Keplerian orbits as long as a state transition matrix can be found.[28] This approach would be faster and more accurate than finding the solution through numerical optimization starting at the circular orbit solution, as in Fig. 11, especially for $e > 0.2$.

## V. Simulation Results

An example is now used to integrate each of the steps of the planner. For this case, the nominal orbit has a semimajor axis and eccentricity of $a = 8378$ km and $e = 0.2$, respectively. There are four satellites in the cluster. The maneuver is defined as a change in formation size and tilt in minimum time. The formation change is written as

$$S_0 = \left\{ \begin{bmatrix} 250 & \text{m} \\ (0, 90, 180, -90) & \text{deg} \\ 0 & \text{m} \\ (0, 90, 180, -90) & \text{deg} \end{bmatrix} \right\} \longrightarrow$$

$$S_F = \left\{ \begin{bmatrix} 300 & \text{m} \\ \alpha_F + (0, 90, 180, -90) & \text{deg} \\ 100 & \text{m} \\ \alpha_F + (0, 90, 180, -90) & \text{deg} \end{bmatrix} \right\} \tag{46}$$

The satellites are not to fall within 50 m of each other.

The planner steps for SA are specifically listed as follows:

1) Minimum-time maneuvers are generated for each satellite with 1-deg increments, or $\alpha_F = 0, 1, \ldots, 359$ deg, using a circular orbit as a reference. A total of $360 \times 4 = 1440$ time-optimal control problems are solved. The final time for the maneuver of each satellite is identical to those shown in Fig. 8. For the cross-axis maneuver, the final time is less than the in-plane final time for all four cases. Therefore, the cross-axis solution does not affect the final time, but does add to the fuel consumption.

2) Collision estimation is evaluated for the cluster optimal case, and a collision proximity of 161 m is found. A scaling of $\sigma_{ca} = 28$ can be used by each satellite to further optimize its maneuver.

3) No CA maneuvers are required to be generated.

4) A table is generated that includes the fuel used for each satellite and each maneuver and the proximity to collision.

5) Final position assignments are evaluated based on minimizing the cluster time subject to collision and propulsion constraints; the cluster minimum time is identical to that shown as the dark solid line in Fig. 8. The cluster minimum time (0.499 orbits) occurs at approximately $\alpha_F = -7$ deg. The phasing of the other satellites are then at 90-deg increments from this angle, as in Eq. (37).

The steps for FG are as follows:

1) Final positions, maneuver switch times, and collision proximity requirements are delivered to each satellite.

2) Based on the switch times from the chosen maneuver, a final maneuver is generated by optimizing the switch times using more complex models with $J_2$ and eccentricity effects. The stable formations are defined for an eccentric orbit using Eq. (6) with $e = 0.2$.

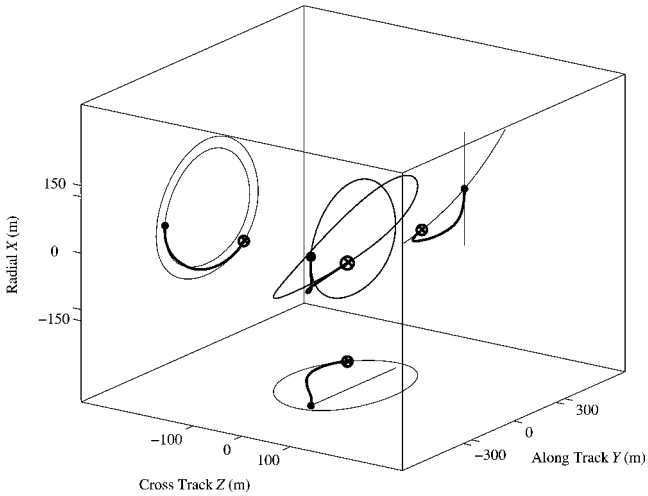


**Fig. 12 Single-satellite reconfiguration maneuver from shown in three-dimensional view (with two-dimensional projections) for an eccentric orbit ($e = 0.2$).**

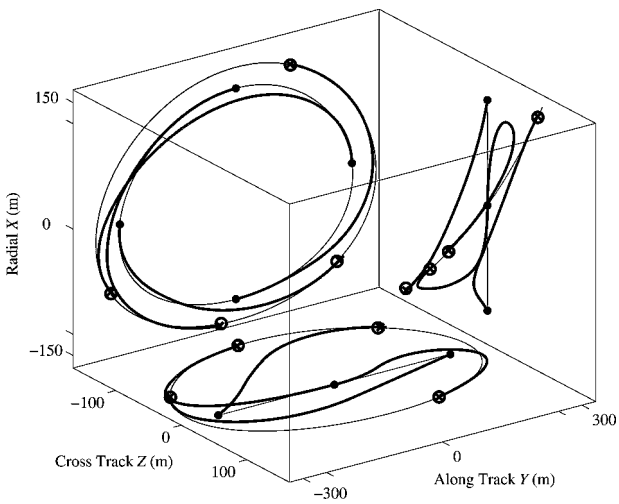


**Fig. 13 Four-satellite cluster reconfiguration maneuver, shown in three dimensions, for an eccentric orbit ($e = 0.2$).**

3) Each individual satellite can replan to optimize other local parameters such that time and collision constraints are not violated ($\sigma_{ca} = 28$). This was not included in the example.

Figure 12 shows a three-dimensional view (with two-dimensional projections) of the second satellite in the formation, $[\alpha_0]_2 = 90$ deg, $[\alpha_F]_2 = 83$ deg. Notice the slightly nonelliptical shape of the initial and final stable formations, as well as the change in tilt. The satellite maneuvers from the initial to final stable formation in approximately half an orbit. Figure 13 shows a summary of all four satellites and their maneuvers from a slightly different view such that the formation tilt can be easily seen. Overall, the maneuver results are quite accurate, even for this eccentric orbit.

Attempting to distribute the approach as much as possible, note that all steps except SA 2–4 can be accomplished in parallel on each individual satellite. When the numerical optimization only is considered, 360 $\mathcal{O}(n^2)$ calculations are made, where $n = 6$ for minimum-time maneuvers and $n = 9$ for minimum-fuel maneuvers. Communication at the leader satellite (the highest bandwidth case because it includes the fleet planner) includes $360 \times 3 = 1080$ data products sent in (time/fuel maps for three other satellites), and two data products sent out (a maneuver selection phasing and collision bound scaling). Fully centralizing this process requires $360 \times 4 = 1440$ $\mathcal{O}(n^2)$ calculations within the fleet planner, and 6 or 9 data products sent out (the switch times for the minimum-time/fuel maneuvers). As a comparison, developing a minimum-time/fuel map using an LP at 360 points for four satellites requires $360 \times 4 = 1440$ $\mathcal{O}(n^3)$ calculations, where $n$ is the number of time-based discretization steps.

## VI. Conclusions

A generalized multiple-satellite planning methodology for clusters has been presented. The algorithm is designed to scale well with number of satellites by easily allowing parallel computations. Many maneuvers are generated using the time- or fuel-optimal problems, based on sets of initial and final conditions. Solutions to the optimal control problems are found using a computationally reliable gradient search mechanism. The minimum time algorithm uses three switch times in the in-plane case and one switch time in the cross-axis case; minimizing the final time as a function of final phasing uses only two switch times in the in-plane case. The minimum-fuel algorithm uses six switch times in the in-plane case, and two in the cross-axis case. The methodology does not overly burden the communications link because only switch times and collision constraints are distributed by the fleet planner. Collisions are avoided by delaying or moving up initial and/or final times. Simulation results on a four-satellite system ($e = 0.2$) show the planner methodology to distribute computations quite well and to be very reliable in its convergence to a cluster-based time or fuel minimum.

## Acknowledgments

This work was supported by the NASA Cross Enterprise Technology Development Program, NASA Grant NAGS-10440, with NASA Goddard Space Flight Center and Neil Dennehy as Program Monitor.

## References

[1]Capps, R. W. (ed.)., *Recommendations for Technology Development and Validation Activities in Support of the Origins Program*," NASA-CR-203426, JPL-PUBL-96-21, June 1996.

[2]Das, A., Cobb, R., and Stallard, M., "TechSat21—A Revolutionary Concept in Distributed Space Based Sensing," AIAA Paper 98-5255, Sept. 1998, pp. 1–6.

[3]Corazzini, T., Robertson, A., Adams, J. C., Hassibi, A., and How, J. P., "GPS Sensing for Spacecraft Formation Flying," *Journal of the Institute of Navigation*, Vol. 45, No. 3, 1998, pp. 195–208.

[4]Purcell, G., Kuang, D., Lichten, S., Wu, S.-C., and Young, L., "Autonomous Formation Flyer (AFF) Sensor Technology Development," *AAS Rocky Mountain Guidance and Control Conference*, Vol. 98, Univelt, Inc., San Diego, CA, 1998, pp. 463–481.

[5]Campbell, M., and Udrea, B., "Collision Avoidance in Satellite Clusters," *2002 American Control Conference*, Inst. of Electrical and Electronics Engineers, Piscataway, NJ, 2002, pp. 1686–1692.

[6]Spores, R., Spanjers, G., Birkan, M., and Lawrence, T., "Overview of the USAF Electric Propulsion Program," AIAA Paper 2001-3225, July 2001.

[7]Rayburn, C., Campbell, M., Hoskins, A., and Cassady, J., "Development of a Micro-PPT for the Dawgstar Nanosatellite," AIAA Paper 2000-3256, July 2000.

[8]Stadter, P., "Confluence of Navigation, Communication, and Control in Distributed Satellite Systems," *IEEE Aerospace Conference*, Inst. of Electrical and Electronics Engineers, Piscataway, NJ, 2001, pp. 26–32.

[9]Zetocha, P., and Brito, M., "Development of a Testbed for Distributed Satellite Command and Control," *IEEE Aerospace Conference*, Inst. of Electrical and Electronics Engineers, Piscataway, NJ, 2001, pp. 609–614.

[10]Schetter, T., Campbell, M., and Surka, D., "Multiple Agent-Based Autonomy for Satellite Constellations," *Lecture Notes in Computer Science*, Vol. 1882, Springer-Verlag, Berlin, 2000, pp. 151–165.

[11]Vadali, S. R., Vaddi, S. S., Naik, K., and Alfriend, K. T., "Control of Satellite Formations," AIAA Paper 2001-4028, Aug. 2001.

[12]Tillerson, M., Inalhan, G., and How, J. P., "Coordination and Control of Distributed Spacecraft Systems Using Convex Optimization Techniques," *International Journal on Nonlinear and Robust Control*, Vol. 12, No. 2–3, 2002, pp. 207–242.

[13]Leitner, J., Bauer, F., Folta, D., Moreau, M., Carpenter, R., and How, J., "Formation Flight in Space," *GPS World*, Vol. 13, Feb. 2002, pp. 22–31.

[14]Carpenter, R., "Decentralized Control of Satellite Clusters," *International Journal on Nonlinear and Robust Control*, Vol. 12, No. 2–3, 2002, pp. 141–161.

[15]Koon, W. S., Marsden, J. E., Murray, R. M., and Masdemont, J., "$J_2$ Dynamics and Formation Flight," AIAA Paper 2001-4090, Aug. 2001.

[16]Yang, G., Yang, Q., Kapila, V., Palmer, D., and Vaidyanathan, R., "Fuel Optimal Maneuvers for Multiple Spacecraft Formation Reconfiguration using Multi-Agent Optimization," *International Journal on Nonlinear and Robust Control*, Vol. 12, No. 2–3, 2002, pp. 243–283.

[17]Wiesel, W. E. (ed.), *Spaceflight Dynamics*, 2nd ed., McGraw–Hill, New York, 1989, pp. 80–85.

[18]Carter, T., and Humi, M., "Fuel-Optimal Rendezvous for Linearized Equations of Motion," *Journal of Guidance, Control, and Dynamics*, Vol. 15, No. 6, 1987, pp. 567–573.

[19]Inalhan, G., Tillerson, M., and How, J. P., "Relative Dynamics and Control of Spacecraft Formations in Eccentric Orbits," *Journal of Guidance, Control, and Dynamics*, Vol. 25, No. 1, 2002, pp. 48–59.

[20]Sedwick, R., Kong, E., and Miller, D., "Exploiting Orbital Dynamics and Micropropulsion for Aperture Synthesis Using Distributed Satellite Systems: Applications to Techsat21," AIAA Paper 98-5289, Oct. 1998.

[21]Schaub, H., and Alfriend, K., "$J_2$ Invariant Orbits for Spacecraft Formations," *Celestial Mechanics and Dynamical Astronomy*, Vol. 79, No. 2, 2001, pp. 77–95.

[22]Lawden, D. F., *Optimal Trajectories for Space Navigation*, Butterworths, London, 1963, pp. 76–81.

[23]Bryson, A., *Control of Spacecraft and Aircraft*, Princeton Univ. Press, Princeton, NJ, 1994, pp. 103–113.

[24]Kirk, D. E., *Optimal Control Theory: An Introduction*, Prentice–Hall, Upper Saddle River, NJ, 1970, pp. 240–258.

[25]Singh, G., Kabamba, P. T., and McClamroch, N. H., "Planar, Time Optimal, Rest to Rest Slewing Maneuvers of Flexible Spacecraft," *Journal of Guidance, Control, and Dynamics*, Vol. 12, No. 1, 1989, pp. 71–81.

[26]Pao, L. Y., and Franklin, G. F., "Time-Optimal Control of Flexible Structures," *Proceedings 1990 Confererence on Decision and Control*, Inst. of Electrical and Electronics Engineers, Piscataway, NJ, 1990, pp. 2580, 2581.

[27]Kurzhanski, A., and Valyi, I., *Ellipsoidal Calculus for Estimation and Control*, Birkauser, Boston, 1997, pp. 104–120.

[28]Carter, T., "State Transition Matrices for Terminal Rendezvous Studies: Brief Survey and New Example," *Journal of Guidance, Control, and Dynamics*, Vol. 21, No. 1, 1998, pp. 148–155.